Available online at www.sciencedirect.com
SCIENCE DIRECT
Polymer 45 (2004) 7767–7777
polymer
www.elsevier.com/locate/polymer

Morphological features and mechanical behavior of one- and two-phase polymeric materials simulated by molecular dynamics

Ricardo Simões[a,b,*], António M. Cunha[a], Witold Brostow[b]

[a]Department of Polymer Engineering, University of Minho, Campus de Azurem, 4800-058 Guimarães, Portugal
[b]Laboratory of Advanced Polymers and Optimized Materials (LAPOM), University of North Texas, Denton, TX 76203-5310, USA

Received 13 July 2004; received in revised form 28 August 2004; accepted 29 August 2004
Available online 11 September 2004

Abstract

Single phase amorphous polymeric materials and two-phase polymer liquid crystals (PLCs) have been created on the computer and their behavior simulated using molecular dynamics. An external force was applied on the material and its response computed along time. The influence of several parameters was investigated, such as the concentration of the rigid LC second phase and the existence of regions of different orientation across the thickness of the material.

A simplified 3-region model, such as that used to model the skin-core structure resulting from injection molding, was used. The influence of the relative size of each region with different properties was determined. Thicker skin regions increase the rigidity of the material, due to their higher orientation in the direction of force application. The concentration of the reinforcing LC second phase has a similar effect, also resulting in a more brittle behavior. The simulations have provided a better understanding of these phenomena.

A method for calculating the true stress during simulation of computer-generated materials (CGMs) is proposed. The true stress behavior was found to differ qualitatively from the engineering stress when the structure of the material allows for considerable changes in cross-sectional area at large-scale deformation.

Keywords: Molecular dynamics; Modeling and simulation; Polymers

1. Introduction

Computer simulations have been previously employed to study a variety of phenomena occurring at the molecular level in polymeric materials [1–3]. These simulations aim at characterizing the behavior and performance of both single-phase amorphous polymers and two-phase polymer liquid crystals (PLCs) under an external uniaxial tensile force. The present paper reports on results from a simple model for addressing the behavior of the typical skin-core microstructure resulting from some processing methods for thermoplastics. More complex models are proposed and will be applied in future simulations.

Polymer liquid crystals are typically copolymers consisting of rigid liquid crystalline (LC) sequences combined with flexible sequences [4] and exhibit a series of improved properties when compared to other polymers [5–7]. Due to the complexity of their behavior, they have been concomitantly studied by statistical mechanics [8,9], viscoelastic models [10–12], and experimental methods [4–7]. However, these research methods have not been able to provide complete answers to some of the pertinent questions about the properties and behavior of these materials. Computer simulations of PLCs can provide information from which those answers might emerge.

Injection molding (IM) is one of the most important processing technologies for thermoplastic materials, namely for parts with a complex geometry. It involves the material flow under high shear and extensional stress fields and high cooling rates that subject the material to a complex thermomechanical environment. Due to all these effects, thermoplastic IM parts exhibit an array of morphological

* Corresponding author. Address: Department of Polymer Engineering, University of Minho, Campus de Azurem, 4800-058 Guimarães, Portugal. Tel.: +351-253510320; fax: +351-253510339.
E-mail addresses: rsimoes@dep.uminho.pt (R. Simões), amcunha@dep.uminho.pt (A.M. Cunha), brostow@unt.edu (W. Brostow).

0032-3861/$ - see front matter © 2004 Elsevier Ltd. All rights reserved.
doi:10.1016/j.polymer.2004.08.063

features through their thickness. This anisotropic layered structure is often simplified to a skin-core model with three regions, two external highly oriented skin regions and an inner spherulitic core, proposed by Tadmor [13]. Although the number of identified layers is dependent on the observer's criteria and the level of detail of the experimental analysis technique employed, the three-layer model has been successfully applied by several authors [14–17] to the study of the influence of morphology on mechanical properties.

Each region in this skin-core layered structure exhibits distinct behavior. The particular morphology of each region and the skin-core ratio (usually defined either in terms of two-dimensional width or area) depend on the specific thermo-mechanical environment during processing. Necessarily, these factors determine the final properties of the molded part. Experimentally, the formation of the skin was found to be thermally controlled at high temperatures and governed by the shear stress level at lower temperatures [17,18].

The skin layer is formed due to the rapid cooling of the hot melt against the cold mold wall during the filling stage. Due to the high orientation of the chains in the melt at this stage, the frozen skin layer displays high degree of orientation. Although Zipper [19] showed that the highly oriented molecular chains in the skin are tilted towards the core and not parallel to the surface of the mold as could be initially assumed, the simplified three-layer model used in the present work will consider the chains in the skin to be parallel to the surface. Future work will improve on this concept and use a more accurate model. The thickness of the skin layer depends not only on the thermomechanical environment (cooling rate, stress fields) but also on the molecular weight of the chains, with higher molecular weights resulting in thicker skins [18].

Due to the insulation effect of the previously formed skin, the low thermal conductivity of polymers and the originally lower shear level, the core material has enough time to undergo an extensive relaxation process—resulting in lower orientation of the core region compared to the skin region. Some models consider the core nearly isotropic as a simplification. Since the present work deals with amorphous materials, the core region will be assumed isotropic.

As pointed out before, computer simulations can provide information to complement experimental results and provide insights into phenomena that cannot be reproduced experimentally, and are not performed with the intent of replacing experimental testing. The concomitant use of simulations and experiments is expected to produce a synergistic effect, resulting in an improved understanding of the properties and behavior of polymeric materials.

2. Simulation method

The statistical segment model of an amorphous polymeric chain has been used, as advocated by Flory [20]. In the statistical segment model, several repeating units of a chain are simplified as one single segment. The creation of materials on the computer is described in Section 3.

The segments interact with each other according to a series of interaction potentials. These differ for intra-chain chemical bonding and inter-chain secondary interactions. Since these simulations deal with both one- and two-phase systems, different potentials were defined to characterize the interactions between segments of the flexible polymer matrix and those of a rigid liquid-crystalline (LC) second phase. The intra-chain bonds between rigid LC segments are represented by a narrow Morse-like potential, allowing only very small bond extensions. In the case of the intra-chain bonds between flexible segments, a spliced double-well potential is used to allow for conformation transitions as in real polymer chains. For both flexible and rigid segments, the inter-chain (secondary) van der Walls interactions are much weaker and are described by Morse-like potentials with a relatively broad well. A detailed description of the potentials has been provided in Ref. [1].

The molecular dynamics (MD) method has been employed to perform the simulations. The preference over alternative methods, such as Monte Carlo (MC) or Brownian dynamics, has been explained elsewhere [1,2]. The time evolution calculation uses a leap-frog algorithm [21].

The MD method considers a system of N particles (statistical segments in this case) evolving along time. Each particle is described by three Cartesian coordinates and three momentum components along the main axes. As these six variables are calculated at each time step of the simulation, the method provides detailed time-dependent behavior for every segment in the system. The major difference between MD and MC is that in MD all particles are moved at once at each time step, whereas in traditional MC each particle moves at a time and that movement is accepted or rejected. In the MD method, time is an explicit variable, which allows the simulation of time-dependent phenomena as well as equilibrium properties. This feature is particularly important in the study of viscoelastic materials.

The molecular dynamics (MD) method has been used for many years to study phenomena which are inaccessible experimentally, or which are too costly to perform [22]. Other significant advantages of computer simulation methods are the ability to study the response under hypothetical conditions which cannot be reproduced in a laboratory, and being able to study variables independently of one another. A detailed review of the various computer simulation methods has been provided by Fossey [22].

MD methods have been employed in the investigation of a wide variety of phenomena in different research areas. Among these is the use of MD by Smith et al. [23] to simulate the X-ray scattering pattern. On the topic of tribology, Gerde and Marder [24] have investigated friction, including its connection to the crack healing mechanism. Theodorou et al. have applied both MC and MD to

investigate a plethora of phenomena, such as diffusion [25], permeation [26], elongational flow [27], and stress relaxation [28]. However, they follow a quite different approach to the problem, performing simulations mostly at the atomistic level, whereas the present study employs a course-grain approach. MD simulations have also been applied to investigate thermal properties and the melting phenomena, including that of thin layers on a substrate [29,30], and the thermodynamic properties of simple fluids and polymer melts [31,32]. Diffusion coefficients of gases through polymers [33] and the transport of fluids through polymer membranes [34] have also been addressed through MD simulations.

Another method of interest for the study of polymers is the kinetic model of fracture, developed by Termonia and co-workers. This method has been successfully employed in the study of the mechanical behavior of polymers [35–37] and the simulation of spider silk fibers [38]. Although focused on phenomena occurring at significant different length scales from those in the present study, fracture mechanics approaches have also been employed in the simulation of polymers [39–42].

The simulation method used in the present paper had been previously applied to the study of stress relaxation in metals and polymers [43–45]. Those simulations have shown that stress relaxation is mainly achieved by plastic deformation occurring in the vicinity of defects. In an ideal lattice, the force required to initiate a crack is higher, but then the force is sufficient to cause quick propagation. A close similarity was found between the stress-relaxation curves resulting from the computer simulations and those from experiments. The simulation results also fit with the Kubát cooperative theory of stress relaxation in materials.

This paper follows simulation work focused on investigating the mechanical properties [1] and the crack formation and propagation phenomena in PLCs [2]. Two of the key questions are *where cracks form* in the material and *how they propagate*, since they could have equally been expected to form in the flexible matrix because of its relative weakness or inside the second phase because of their relative rigidity. Based on simulation results, it was shown that cracks appear preferentially between regions where agglomerates of the second phase exist in close proximity. The cracks then grow along the interface of the two phases. Whenever that preferential crack growth path is unavailable, cracks will propagate through the flexible phase.

More recently, a similar simulation method was employed in the study of tribological properties, namely scratch resistance and recovery of amorphous polymeric materials [3]. Although at a preliminary stage, these simulations indicate that the tribological properties are mainly dictated by the local chain geometry. In the case of two-phase PLCs, performance can be improved if the rigid second phase exhibits preferential migration to the surface.

3. Material generation procedures

3.1. Single-region materials

Both one- and two-phase polymeric materials were created on the computer. In each of these cases, the amorphous phase is comprised of a series of self-avoiding coiled chains. For two-phase materials, a rigid LC phase is then dispersed in the flexible matrix up to a specified concentration.

The creation of the coiled chains follows a procedure developed by Mom [46] and later modified to result in a more realistic representation of polymeric chains [47]. All segments in the material are initially positioned in a triangular lattice, filling all available positions. At this stage, each segment represents one chain of length 1. The reasons for using the triangular lattice have been previously discussed [43,47], but the main reason is the more realistic coordination number than, for example, that of the square lattice. Following this procedure, both completely filled lattices and those containing vacancies can be created.

Chains grow along time by bonding of neighboring end-of-chain segments, similarly to the step-wise polymerization process. Whenever several pairs of segments are equally spaced, which happens very frequently in the early stages of the procedure, one of these pairs is randomly picked, and the segments bond to form a chain of length 2. This mechanism is then repeated until no more segments can be bonded in this way. A preferential direction can be defined for chain growth, originating structures with varying degrees of orientation along the main axes. However, in the present work this feature was not used and the amorphous phase is always randomly oriented. Even though the procedure for chain growth is relatively simple, the resulting three-dimensional materials exhibit several realistic features, as previously described in Ref. [47].

In the case of two-phase polymer liquid crystals (PLCs), the LC reinforcement is then added to the flexible matrix. Experimental data clearly shows that the LC phase forms quasi-spherical agglomerates [48,49], usually called islands. Thus, in order to achieve the desired LC concentration, islands of a chosen size are introduced in the CGM by random sequential addition.

To determine the influence of the LC concentration on the properties and behavior of the CGMs, as discussed in Section 5.2, it was essential that the effects of the chain geometry and island spatial distribution were prevented, since these have been previously shown to affect the mechanical response of the material [2,50]. Thus, for creating the materials described in Section 5.2, an approach that isolates the influence of the LC concentration was employed. Instead of independently creating materials with varying LC concentration, a CGM containing the highest LC concentration of interest is created first and then islands are randomly removed to obtain lower concentration

materials. In this way, the chain geometry and island spatial distribution are kept constant.

As the islands are placed in random positions in the material, it is common to find in a CGM some regions with high local concentration surrounded by regions of lower concentration. As could be expected, this distribution of the islands greatly influences the crack initiation and crack propagation phenomena [2]. Simulations were also used to investigate the influence of the size of the LC islands. At least within the studied size range, the island size did not significantly affect the properties, and had a negligible effect during the early stages of the simulation [50]. However, it does seem to affect the large-scale deformation process as well as the cracking phenomena.

A detailed description of the material generation procedure has been previously provided [47], together with an analysis of the resulting three-dimensional CGMs.

3.2. Multi-region materials

As previously discussed, IM thermoplastic parts exhibit a skin-core pattern, due to rapid cooling of material directly in contact with the cold mold walls. In order to represent such materials on the computer, multiple regions inside a CGM have been considered. The term *skin region* is used when referring to regions of aligned chains, which can be aligned with an axis or slanted at a certain angle. The term *core region* is used when referring to regions of coiled chains (for any degree of orientation chosen).

The skin ratio (S_r) was defined as the breadth of the skin region divided by the total breadth, or in other words, the number of lattice rows of the skin region divided by the total number of lattice rows.

The creation of core regions follows the procedure described in Section 3.1. Although the orientation of the amorphous chains could be controlled by specifying a desired value of the probability of alignment of each bond with a certain axis, the simulations discussed in the present paper were performed with completely isotropic core and completely aligned skin. The skin is created following an analogous procedure but now the bonds can only form along a preferential direction, the x-axis in this case.

Two optimization algorithms have also been developed to allow more flexibility to the generation process. A detailed description of these has been provided elsewhere [47].

An example of a 5-region material created using this procedure is shown in Fig. 1. The regions are, from top to bottom, skin 100% oriented with the x-axis, slanted skin at 120° with the x-axis, randomly oriented core, slanted skin at 60° with the x-axis, and skin 100% oriented with the x-axis.

4. Simulation details

The CGM creation process, described in Section 3, is based on placing segments in lattice positions. This

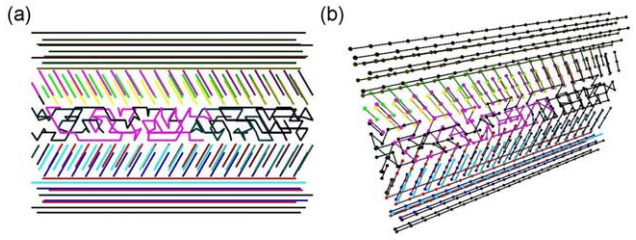

Fig. 1. (a) Five-region material within a simulation cell containing approximately 900 statistical segments. Each chain is represented in a different color for ease of visualization; (b) another view of this material with segments shown as spheres.

corresponds to an idealized structure with all bonds in a non-strained state. A random perturbation is introduced in the beginning of the simulation procedure by slightly shifting the position of all segments by a small random value (less than 1% of the equilibrium distance between segments). Then, the first simulation step is run with no external forces applied to allow the system to reach equilibrium.

After that stage, a uniaxial external tensile force is applied to the edges of the material along the x-axis. The value of the external force starts at zero and increases by the same amount at every simulation step until fracture of the material is observed.

The shape of the CGM changes along the three Cartesian axes during the simulation, depending on the loading conditions and the structure of the material. Thus, the engineering stress is no longer an accurate measure of the mechanical environment the material is being subjected to. In order to calculate the true stress on the material, it is divided into 10 sections along the x-axis (although this number could be easily changed to accommodate materials of significantly different size), and the geometry of each section is monitored along time. Since the deformation is clearly non-homogeneous, with both localized necking and crack formation occurring under different conditions, abrupt changes in the true stress behavior are often observed.

In these simulations the force is always applied along the x-axis, and thus, the cross-section is defined in the y–z plane. All sections are initially parallelepipeds of equal size, except for the last section, which depends on the exact number of columns in the material. Each section is defined by the positions of the segments at their eight corners. These segments are assigned to each section in the beginning of the simulation, and their change in position along time determines the geometry of the sections. The initial division of the material in sections and the definition of a section are shown in Fig. 2.

Each section can be characterized by two cross-sectional areas, one defined by the leftmost segments and the other defined by the rightmost segments along the x-axis. These two areas are labeled A_l and A_r in Fig. 2. An average cross-sectional area is then calculated for each section simply as the average of A_l and A_r. The true stress σ_t is calculated

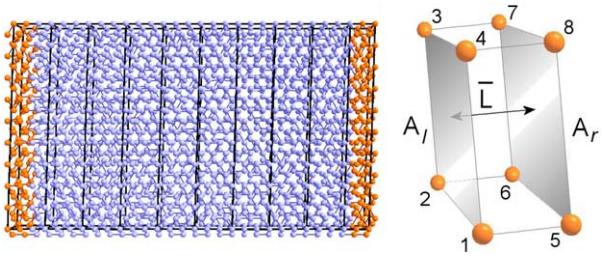

Fig. 2. Sections used in the CGM to compute the true stress.

based on the minimum average cross-sectional area of all sections:

$$\sigma_t = \frac{F_{ext}}{\min\{\bar{A}_1, \bar{A}_2, \ldots, \bar{A}_{10}\}} \quad (1)$$

There are some unavoidable approximations involved in this analysis: segments intersected by the boundary between two sections are considered as belonging to only one of them, and a small number of segments sometimes escape the overall boundaries of all sections. These effects have been thoroughly tested and present a negligible effect on the final results. When the system reaches large-scale deformation, however, the shape of the sections sometimes becomes inadequate for calculating the cross-sectional area. In this case, the user must determine up to which simulation step the values of the true stress should be considered.

Since these simulations deal with phenomena at a macromolecular level, the use of the general concept of macroscopic strain at this scale is arguable. However, by applying again the sections concept, the strain is calculated from the distance between the leftmost and rightmost cross-sectional areas of the material, that is, A_l of section 1 and A_r of section 10. Although typically it would be of interest to measure the strain at break as a material property, the random nature of the cracking phenomena makes it more useful in some cases to measure the strain at a certain time into the simulation. Since all simulations are performed with the same loading conditions, that measurement is representative of the mechanical history on the sample and provides a qualitative indicator of the material response.

A system of coherent dimensionless units is used in these simulations, as previously described [1]. The length of a non-strained bond corresponds to a unit of length, the mass of a statistical segment corresponds to a unit of mass, and the energy needed to dissociate a bond corresponds to a unit of energy. Thus, a unit of force is given by the ratio of one unit of energy to one unit of length. Other quantities can be similarly defined.

5. Selected results

The skin ratio and the concentration of the rigid LC second phase have been varied to observe the effects on the properties of the material. All the CGMs discussed in this section were created within a simulation cell containing approximately 2400 statistical segments. A single simulation was run for each set of conditions. This was mainly imposed by the computation time required for each simulation. The variability of results from several simulations with the same set of conditions was confirmed to be small enough not to affect the overall results discussed in this paper.

Five values of the skin ratio S_r were used, varying between 0 (single-core region) and 1 (single-skin region) in equal intervals of 0.2. For each S_r, the modulus is calculated from the stress–strain curves using two different methods: the slope of the initial linear region of the curve, defined as the apparent modulus (E_{app}), and a secant modulus at a strain of 0.1 (E_{sec}). In these simulations, the true stress was also determined following the procedure described in Section 4.

Section 5.1 describes results for a fully flexible material. The results for the two-phase materials, respectively containing 20 and 30% LC phase, are discussed in Section 5.2. This analysis allows investigation of the effect of the skin ratio and simultaneously the effect of the second phase concentration on the properties. Although it would be too extensive to represent the structures of all the simulated CGMs, selected structures are shown in Fig. 3.

5.1. Effect of the skin-core ratio

For perspicuity sake, the behavior of single-region materials, which are the limiting cases, shall be investigated first. After that, the more complex case of three-region models shall be addressed. The stress–strain curves for the skin ratios of 0 (single-core) and 1 (single-skin) are shown respectively in Figs. 4 and 5.

As expected, the skin and the core regions display different behavior. The core material is characterized by large-scale deformation developing along time due to chain motion mechanisms, such as chain unfolding and chain separation. The true stress levels are much higher than the engineering stress, due to significant cross-section reduction during deformation. Moreover, the reduction is not uniform throughout the material, and is dependent on the local chain geometry. The true stress has a higher slope than the engineering stress, which indicates a progressive tendency for the cross-section to decrease with increasing values of the force. This is expected, since large-scale deformation in the direction of force application is accompanied by a decrease in size along the perpendicular directions.

In the skin material, higher values of the true stress are observed compared to the engineering stress. However, in this case, the two curves have a very similar shape. This is due to the fact that in the skin material, all chains are oriented with the direction of force application. Thus, elongation is achieved initially by bond conformation changes, which is accompanied by a decrease in the cross-section. However, after all bonds have changed

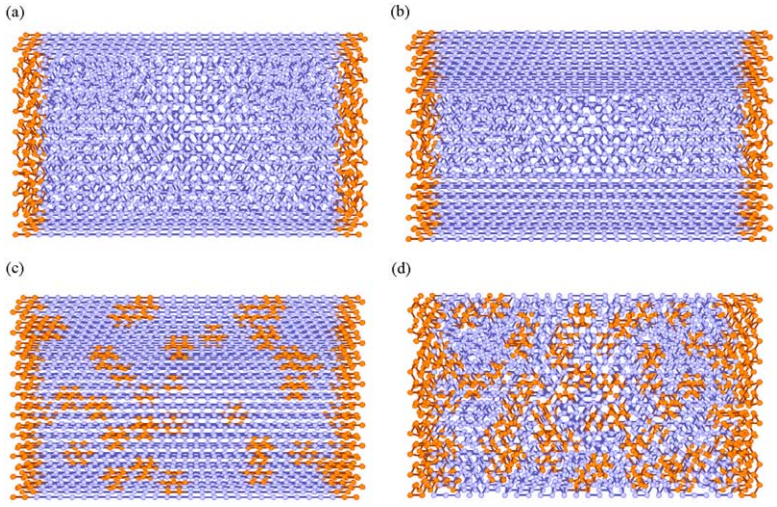

Fig. 3. Examples of CGMs used for simulation: (a) single-phase CGM of $S_r = 0.2$; (b) single-phase CGM of $S_r = 0.6$; (c) two-phase 20% LC CGM of $S_r = 1$; (d) two-phase 30% LC CGM of $S_r = 0$.

conformation, the force continues to increase but the cross-section remains approximately constant up to fracture.

This behavior can also be seen in the two distinct regions of the curve, one similar to the core material and another characterized by a very high slope, where the force increases substantially with very small change of deformation. In the second region, the applied force already caused all bonds to change conformation, but it is not sufficient to break primary bonds in the material. The force keeps increasing up to the point where it can cause primary bond rupture. At that point, the material fractures.

Even though the engineering stress of the skin material is higher than the core material, particularly near fracture, the true stress levels on both materials at fracture are very similar. Although they fail at very different force values, the changes in cross-sectional area are also significantly different, resulting in similar values of true stress at fracture. This is discussed in more detail below.

The evolution of the section geometry along time for the core material is shown in Fig. 6. As explained above, the differences in behavior of the engineering and true stresses can be explained by the significant changes in section geometry during deformation. Moreover, it is clear from this figure that the deformation is non-homogeneous, thus resulting in different values of the cross-sectional area of the sections. For comparison, the case of the skin material is shown in Fig. 7. Although in early stages there is a decrease of the cross-sectional area, it then remains constant for an extended period preceding fracture.

The apparent modulus (E_{app}) and the secant modulus (E_{sec}) are shown in Fig. 8 for each S_r simulated. As expected, there is a general tendency for the modulus to increase with increasing S_r. This is due to the more rigid and brittle behavior of skin regions. Although the two methods of modulus calculation result in different values, the general tendency is similar for both cases. The differences are related to instability of the curves at the initial stages, where deformations are small and the choice of points for modulus calculation influences the results.

The values of the strain at break (ε_b) for varying S_r are shown in Fig. 9. The strain at break tends to decrease with

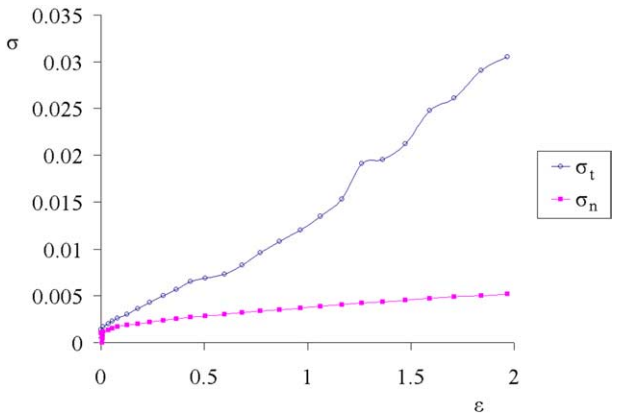

Fig. 4. Stress–strain curve for the case of a single-core region. Here, σ_t is the true stress, σ_n is the engineering stress, and ε is the strain.

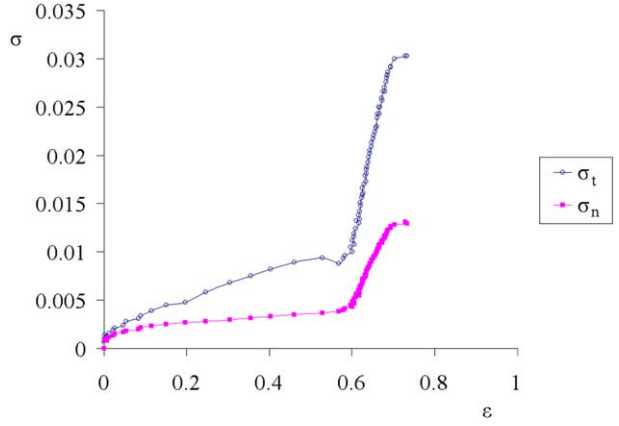

Fig. 5. Stress–strain curve for the case of a single-skin region. Here, σ_t is the true stress, σ_n is the engineering stress, and ε is the strain.

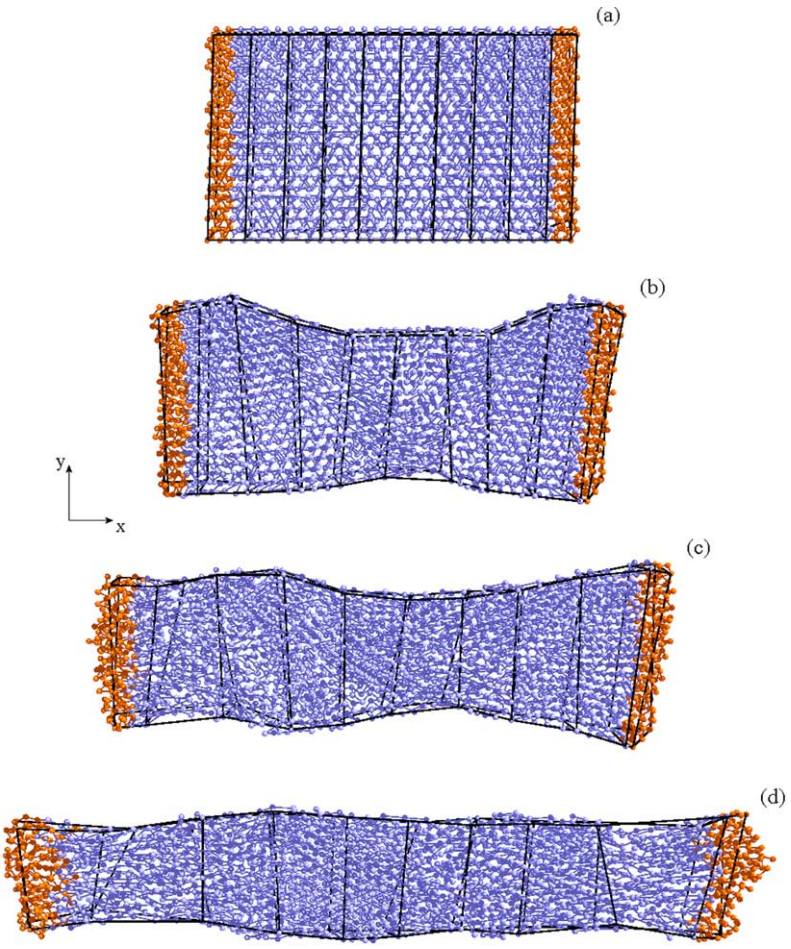

Fig. 6. Changes in the geometry of the sections during deformation of the core material: (a) $t=1$ simulation step; (b) $t=14$ simulation steps; (c) $t=18$ simulation steps; (d) $t=23$ simulation steps.

increasing S_r. As previously stated, the skin regions are more rigid and brittle than the core regions. Therefore, although higher skin ratios exhibit a higher modulus, this also results in fracture at lower deformations. Decreased ductility with increasing degree of orientation has been experimentally observed [14]. A significant decrease of the strain at break with increasing skin thickness was reported for injection-molded polypropylene [51].

From the analysis of Fig. 9(a), the core material seems to have a lower strain at break than materials with S_r of 0.2 and 0.4. This happens because it is very difficult to establish fracture criteria that can be applied to all simulations. Actually, since the core material exhibits large-scale deformation, the bulk of the material does not deform uniformly as the skin material does. It is useful in this case to measure the strain after a certain time for each S_r under equal force conditions. In that case, a more accurate representation of the extent of deformation is obtained, as shown in Fig. 9(b). Note that the time scale is in simulation steps since the status of the material is not recorded every time step, but only every 2000 time steps. Thus, each simulation step corresponds to 2000 time steps. The values of the engineering stress and true stress at break have also been compared for the different S_r; see Fig. 10.

The engineering stress at break does not show a significant dependence on S_r, except for the case of the single-skin region. For that case, the high value is due to the limited chain motion that requires the force to reach values sufficiently high to break primary bonds, as previously explained. The true stress decreases with increasing S_r, since skin regions tend to exhibit smaller changes in the cross-sectional area than core regions. This does not hold for the single-skin region, due to the reasons previously described for the engineering stress. Thus, the global behavior of these materials seems to be mainly determined by the core region. In the single-skin material, the absence of core results in significantly different behavior.

5.2. Effect of the liquid-crystalline (LC) concentration

The differences in the stress–strain behavior for the varying skin ratios of the 20% LC material are shown in Fig. 11. The true stress increases dramatically near fracture, since the cross-sectional area is being significantly

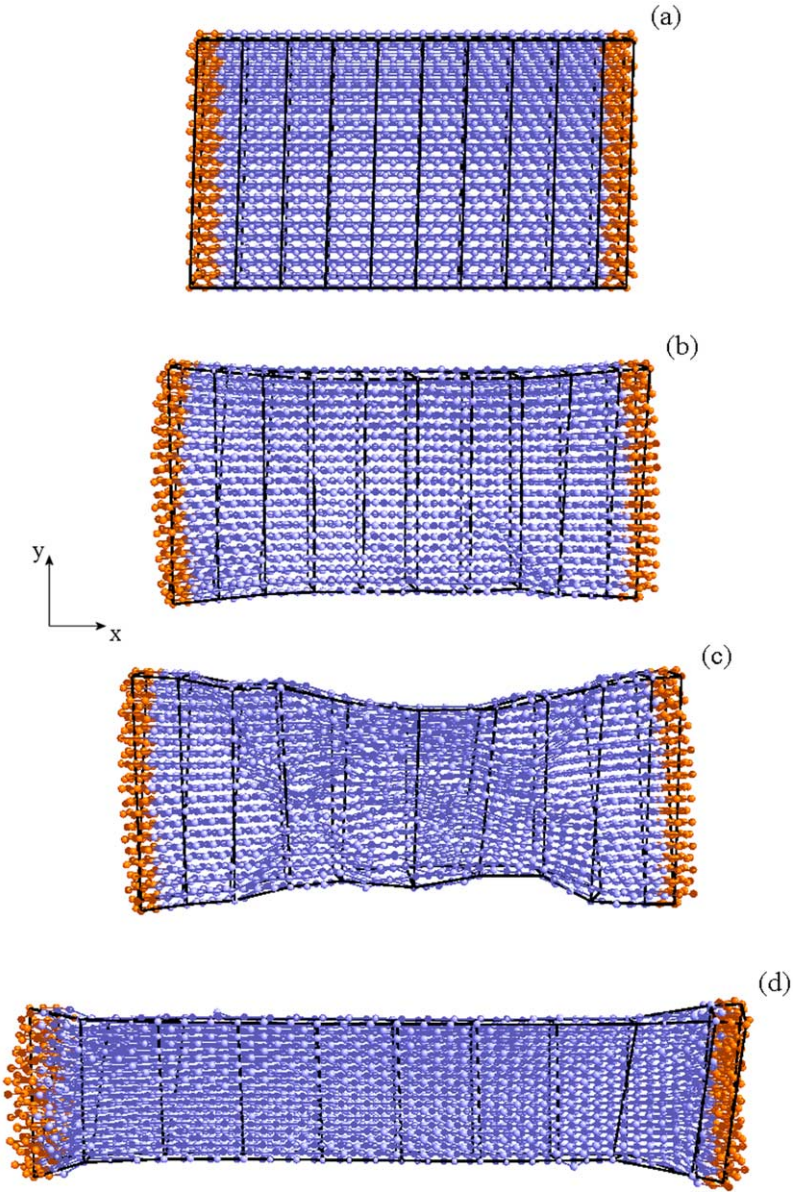

Fig. 7. Changes in the geometry of the sections during deformation of the skin material: (a) $t=1$ simulation step; (b) $t=14$ simulation steps; (c) $t=18$ simulation steps; (d) $t=27$ simulation steps.

decreased. This feature of the curve is also observed in experimental determination of the true stress.

Similarly to the approach discussed in Section 5.1, the skin ratio was varied between 0 and 1 for each LC concentration value. The secant modulus for each of these materials is shown in Fig. 12.

The secant modulus for 20 and 30% LC concentrations shows the same tendency as it did for the flexible material, increasing with S_r. Fig. 12 also shows that increasing LC concentration results in an increase of the modulus. Thus, the second phase is performing its role as reinforcement. For the 30% LC case, the effect is significantly accentuated at high S_r. This is because the predominant deformation mechanism of the skin region, bond conformation change, is highly limited by the large number of islands.

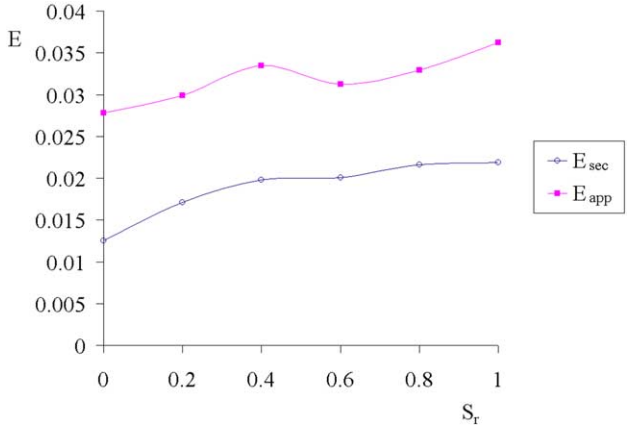

Fig. 8. Effect of the skin ratio (S_r) on the modulus (E). Here, E_{app} is the apparent modulus and E_{sec} is the secant modulus.

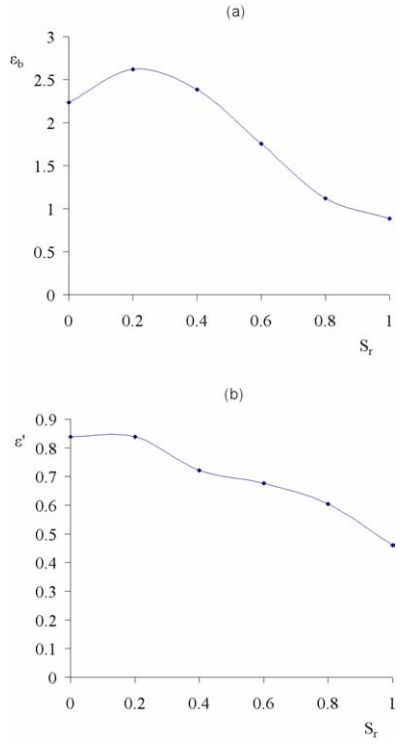

Fig. 9. Strain behavior for different skin ratios (S_r): (a) effect of the skin ratio on the strain at break (ε_b); (b) strain at time $t=20$ simulation steps (ε').

The increased rigidity of the two-phase materials also reflects on the strain behavior. The strain after a certain simulation time can be calculated for all materials and compared with the flexible case. This is shown in Fig. 13.

The strain at time $t=20$ simulation steps decreases with S_r for the two-phase materials similarly to the case of the flexible material. The LC phase also significantly reduces ε'. Note that the values for the skin material containing 30% LC are one order of magnitude lower than for the other materials.

The presence of the LC phase could be expected to equally affect the true stress at break $\sigma_{t,b}$. However, since the presence of LC islands both increases the rigidity of the material and decreases the deformation, thus also limiting the decrease in minimum cross-sectional area, $\sigma_{t,b}$ is not significantly affected except for the limiting cases. This effect is shown in Fig. 14.

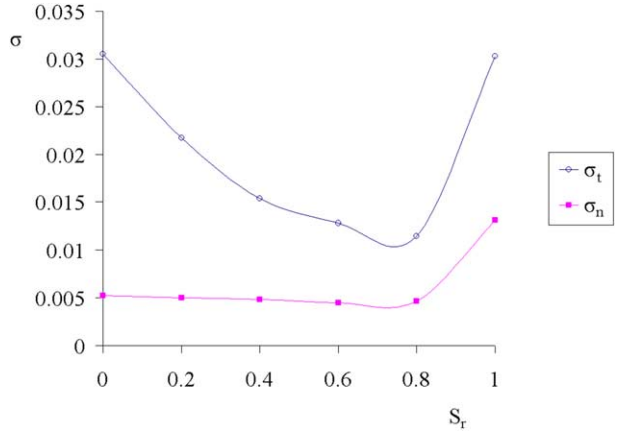

Fig. 10. Effect of the skin ratio (S_r) on the stress at break. Here, σ_t is the true stress and σ_n is the engineering stress.

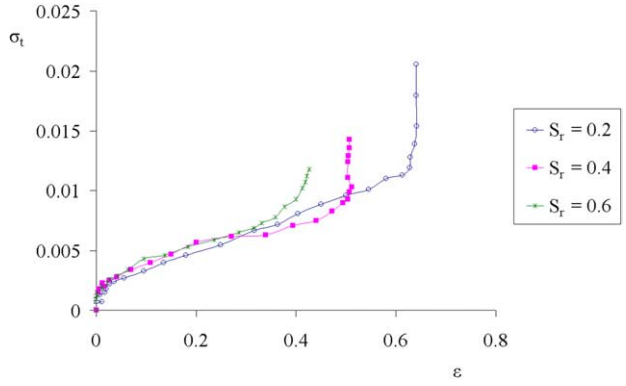

Fig. 11. Effect of the skin ratio (S_r) on the stress–strain behavior of the 20% LC material. Here, σ_t is the true stress and ε is the strain.

For all materials with a skin region, the LC phase actually induces a decrease of the $\sigma_{t,b}$ due to the combined effect of the skin and the islands, that partially prevent the changes in cross-sectional area. However, the core material exhibits increasing $\sigma_{t,b}$ with increase in LC concentration. In this case, the random distribution of the islands causes some regions of the material to deform more and others to deform less. The regions with higher deformation will exhibit significant decrease in cross-sectional area. To better understand this, the minimum cross-sectional area at break (A_{min}) can be compared for the different materials. This is shown in Fig. 15.

6. Concluding remarks

By emulating the step-wise polymerization process, it is possible to create *realistic* polymeric materials on the computer. These materials exhibit the important features of real polymers, such as the end-to-end distance of chains and molecular weight distribution. The software developed also allows control over the morphology of the material, degree

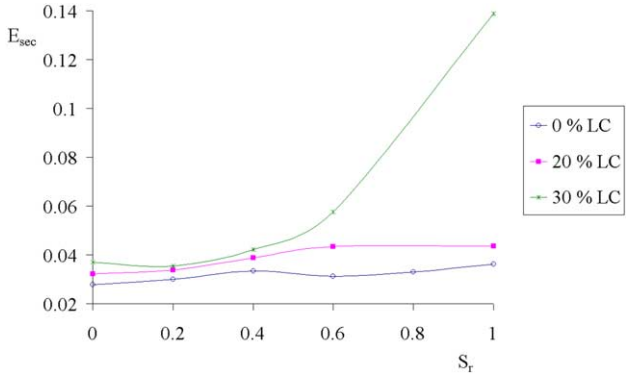

Fig. 12. Effect of the skin ratio (S_r) on the secant modulus (E_{sec}) for different LC concentrations.

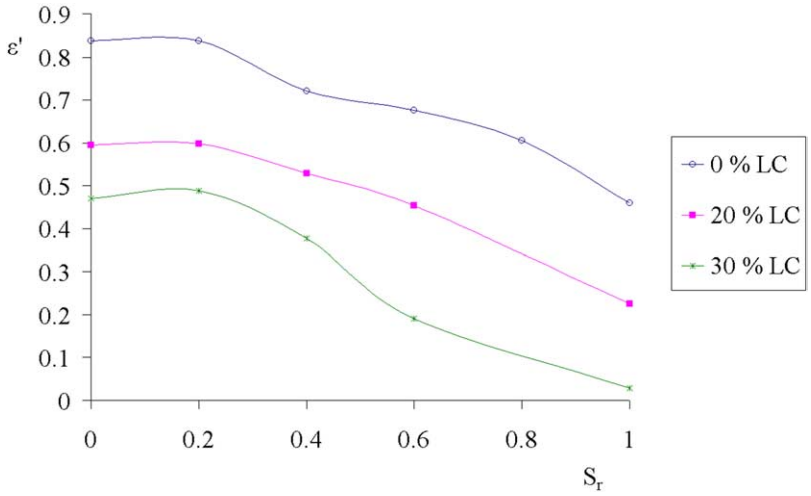

Fig. 13. Strain behavior of materials with different LC concentrations as a function of the skin ratio (S_r). Here, ε' is the strain at time $t=20$ simulation steps.

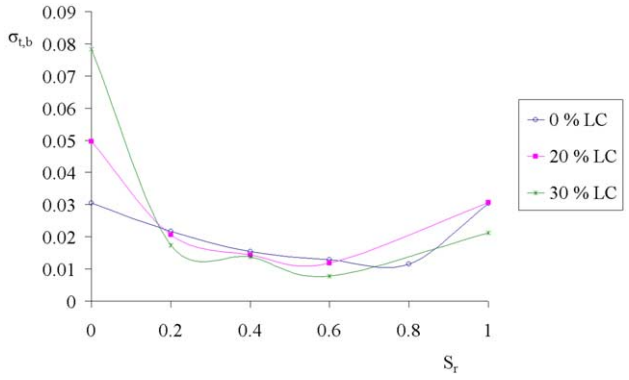

Fig. 14. True stress at break ($\sigma_{t,b}$) of materials with different LC concentrations as a function of the skin ratio (S_r).

of orientation and dispersion of a second phase. In the case of multi-region materials, the relative size of each region can be easily varied and then related to the final properties.

The rigid LC phase indeed performs its role as reinforcement, increasing the modulus of the material; however, it also favors the formation and propagation of cracks. The material becomes stronger but simultaneously more brittle.

True stress calculations have shown how the changes in cross-sectional area result in true stress levels much higher than those indicated by the engineering stress. In this way, a more accurate measure of the mechanical conditions imposed on the material is obtained. Furthermore, the true stress behavior is *qualitatively* different from that of the engineering stress. Since the material often exhibits highly localized deformation, the true stress in a certain region can increase substantially compared to the overall values. In that case, those regions become probable *loci* for failure to occur. This effect also reflects on the free volume measurement for those regions. The free volume affects the mobility of the segments and thus affects the mechanical properties.

Skin-core layered structures have also been studied. The skin and core regions exhibit completely different behavior due to their specific morphologies. Skin regions are

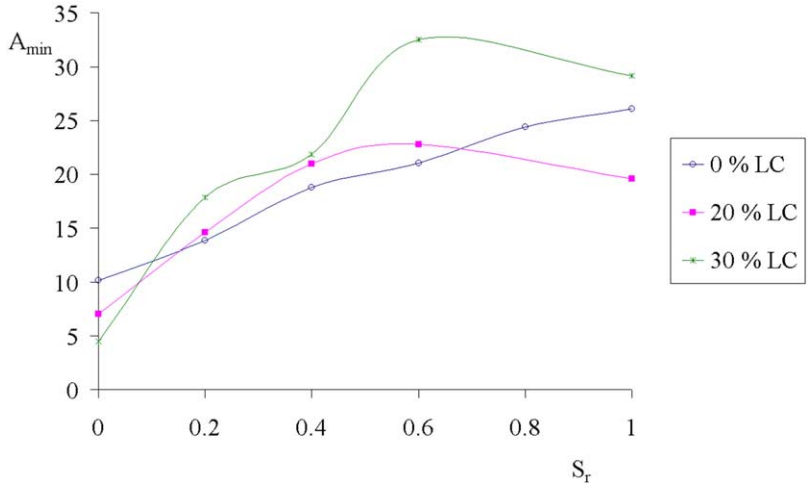

Fig. 15. Minimum cross-sectional area (A_{min}) for materials with different LC concentrations as a function of the skin ratio (S_r).

predominantly brittle and break at relatively low strain values, while core regions are predominantly ductile and have high values of the strain at break. However, both regions were found to fail at similar true stress levels. The skin-core ratio was shown to influence the mechanical properties even if the orientation of each region is kept constant.

In future simulations, a 5-region model can be used, instead of the simplified 3-region model employed thus far. However, in order to expand the model, it is required to experimentally delaminate and analyze each region individually so that the model accurately represents the real structure.

The possibility of predicting the mechanical properties from simulation results is encouraging, but further work is required before quantitative relationships can be established. Although the simulations have provided pertinent information regarding phenomena taking place at the mesoscale, the jump to macroscopic properties and behavior requires additional work.

Acknowledgements

Support for this research has been provided by the Fundação para a Ciência e a Tecnologia, 3° Quadro Comunitário de Apoio, Lisbon, and also by the Robert A. Welch Foundation, Houston (Grant # B-1203).

References

[1] Brostow W, Donahue III M, Karashin CE, Simoes R. Mater Res Innovations 2001;4:75.
[2] Brostow W, Cunha AM, Quintanilla J, Simoes R. Macromol Theory Simul 2002;11:308.
[3] Brostow W, Hinze JA, Simoes R. J Mater Res 2004;19:851.
[4] Samulski ET. Faraday Disc 1985;79:7.
[5] Brostow W. Polymer 1990;31:979.
[6] Brostow W. In: Mark JE, editor. Physical properties of polymers handbook. Woodbury, NY: American Institute of Physics Press; 1996. Chapter 33.
[7] Hess M, Lopez BL. In: Brostow W, editor. Mechanical and thermophysical properties of polymer liquid crystals. London: Chapman & Hall; 1998. Chapter 9.
[8] Brostow W, Hibner K, Walasek J. J Chem Phys 1998;108:6484.
[9] Brostow W, Walasek J. J Chem Phys 2001;114:2466.
[10] Brostow W, D'Souza NA, Kubat J, Maksimov R. J Chem Phys 1999; 110:9706.
[11] Brostow W. Mater Res Innovations 2000;3:347.
[12] Akinay AE, Brostow W. Polymer 2001;42:4527.
[13] Tadmor Z, Gogos GG. Principles of polymer processing. New York: Wiley; 1979.
[14] Cunha AM, Pouzada AS, Crawford RJ. Plast Rubber Compos Process Appl 1992;18:79.
[15] Fujiyama M. In: Karger-Koscis J, editor. Polypropylene structure, blends and composites: structure and morphology, vol. 1. London: Chapman & Hall; 1995. Chapter 6.
[16] Phillips R, Herbert G, News J, Wolkowicz M. Polym Eng Sci 1994; 34:1731.
[17] Viana JC, Cunha AM, Billon N. Int Polym 1997;43:159.
[18] Brito AM, Cunha AM, Pouzada AS, Crawford RJ. Int Polym Proc VI 1991;4:370.
[19] Zipper P, Abuja PM, Janosi A, Wrentschur E, Geymayer W, Ingolic E, et al. Int Polym Proc X 1995;4:341.
[20] Flory PJ. Statistical mechanics of chain molecules. New York: Wiley; 1969.
[21] van Gunsteren WF. In: Truhlar DG, editor. Mathematical frontiers in computational chemical physics. New York: Springer; 1988.
[22] Fossey S. In: Brostow W, editor. Performance of plastics. Munich-Cincinnati: Hanser; 2000. p. 63.
[23] Ayyagari C, Bedrov D, Smith GD. Macromolecules 2000;33:6194.
[24] Gerde E, Marder M. Nature 2001;413:285.
[25] Karayiannis NC, Mavrantzas VG, Theodorou DN. Chem Eng Sci 2001;56:2789.
[26] Makrodimitris K, Papadopoulos GK, Theodorou DN. J Phys Chem B 2001;105:777.
[27] Mavrantzas VG, Theodorou DN. Macromol Theory Simul 2000;9: 500.
[28] Harmandaris VA, Mavrantzas VG, Theodorou DN. Macromolecules 2000;33:8062.
[29] Abraham FF. Phys Rev Lett 1980;44:463.
[30] Abraham FF, Rudge WE, Auerbach DJ, Koch SW. Phys Rev Lett 1984;52:445.
[31] Andersen HC. J Chem Phys 1980;72:2384.
[32] Banaszak M. TASK Quart 2001;5:17.
[33] Muller-Plathe F, Rogers SC, Van Gunsteren WF. Macromolecules 1992;25:6722.
[34] Fritz L, Hofmann D. Polymer 1997;38:1035.
[35] Termonia Y. Encyclopedia of polymer science and technology, 3rd ed. New York: Wiley; 2002.
[36] Termonia Y, Smith P. Macromolecules 1987;20:835.
[37] Termonia Y, Smith P. Macromolecules 1988;21:2184.
[38] Termonia Y. Macromolecules 1994;27:7378.
[39] Karger-Kocsis J. In: Cunha AM, editor. Structure development in processing for polymer property enhancement. Brussels: North Atlantic Treaty Organization; 1999.
[40] Santana OO, Maspoch ML, Martinez AB. Polym Bull 1999;39:511.
[41] Li Y, Ann H, Binienda WK. Int J Solids Struct 1998;11:981.
[42] Shbeeb N, Binienda WK, Kreider K. Int J Fract 2000;104:23.
[43] Brostow W, Kubat J. Phys Rev B 1993;47:7659.
[44] Blonski S, Brostow W, Kubát J. Phys Rev B 1994;49:6494.
[45] Brostow W, Kubát J, Kubát MJ. Mech Compos Mater 1995;31:432.
[46] Mom V. J Comput Chem 1981;2:446.
[47] Brostow W, Cunha AM, Simoes R. Mater Res Innovations 2003;7:19.
[48] Brostow W, Dziemianowicz TS, Romanski R, Werber W. Polym Eng Sci 1988;28:785.
[49] Brostow W, Hess M. Mater Res Soc Symp 1992;255:57.
[50] Brostow W, Cunha AM, Viana JC, Simoes R. Proc Ann Tech Conf Soc Plast Engrs 2003;61:2957.
[51] Pleβmann K, Mendes G, Cremer M, Fenske W, Feser W, Netze C, Offergeld H, Pötsch G, Stabrey H. Kunststoffe 1990;80:200.